High-throughput screening for extracellular inhibitors of the FLT3 receptor tyrosine kinase reveals chemically diverse and druggable negative allosteric modulators

Romain Hany, Jean-Philippe Leyris, Guillaume Bret, Sylvie Mallié, Chamroeun Sar, Maxime Thouaye, Abdallah Hamze, Olivier Provot, Pierre Sokoloff, Jean Valmier, et al.

▶ **To cite this version:**

Romain Hany, Jean-Philippe Leyris, Guillaume Bret, Sylvie Mallié, Chamroeun Sar, et al.. High-throughput screening for extracellular inhibitors of the FLT3 receptor tyrosine kinase reveals chemically diverse and druggable negative allosteric modulators. ACS Chemical Biology, 2022, 17 (3), pp.709-722. 10.1021/acschembio.2c00048 . hal-03747971

HAL Id: hal-03747971
https://hal.science/hal-03747971

Submitted on 9 Aug 2022

HAL is a multi-disciplinary open access archive for the deposit and dissemination of scientific research documents, whether they are published or not. The documents may come from teaching and research institutions in France or abroad, or from public or private research centers.

L'archive ouverte pluridisciplinaire **HAL**, est destinée au dépôt et à la diffusion de documents scientifiques de niveau recherche, publiés ou non, émanant des établissements d'enseignement et de recherche français ou étrangers, des laboratoires publics ou privés.

High-throughput screening for extracellular inhibitors of the FLT3 receptor tyrosine kinase reveals chemically diverse and druggable negative allosteric modulators.

Romain Hany,[†,∞] Jean-Philippe Leyris,[‡,§,≠,∞] Guillaume Bret,[¶] Sylvie Mallié,[‡,§] Chamroeun Sar,[‡,§] Maxime Thouaye,[‡,§] Abdallah Hamze,[Δ] Olivier Provot,[Δ] Pierre Sokoloff,[≠] Jean Valmier,[‡,§,] Pascal Villa[†] and Didier Rognan[¶,*]

[†]Plate-forme de Chimie Biologique Intégrative de Strasbourg (PCBIS), UAR3286 CNRS-Université de Strasbourg, Institut du Médicament de Strasbourg, ESBS Pôle API, Bld Sébastien Brant, 67412 Illkirch Cedex, France

[‡]Institut des Neurosciences de Montpellier (INM), INSERM, Institut National de la Santé et de la Recherche Médicale, UMR1051, Hôpital Saint-Eloi, Montpellier, France.

[§]Université de Montpellier, Montpellier, France.

[Δ] Université Paris-Saclay, CNRS, BioCIS, 92290, Châtenay-Malabry, France

[¶]Laboratoire d'Innovation Thérapeutique (LIT), UMR7200 CNRS-Université de Strasbourg, Illkirch, France

[≠]BIODOL Therapeutics, CAP Alpha, Clapiers, France

[∞]Both authors equally contributed to this work

ABSTRACT

Inhibiting receptor tyrosine kinases is commonly achieved by two main strategies targeting either the intracellular kinase domain by low molecular weight compounds or the extracellular ligand-binding domain by monoclonal antibodies. Identifying small molecules able to inhibit RTKs at the extracellular level would be highly desirable to gain exquisite selectivity but is believed to be challenging owing to the size of RTK endogenous ligands (cytokines, growth factors) and the topology of RTK extracellular domains. We here report the high-throughput screening of the French Chemical Library (48K compounds) for extracellular inhibitors of the Fms-like tyrosine kinase 3 (FLT3) receptor tyrosine kinase, by a homogeneous time-resolved fluorescence competition assay. 679 small molecular weight ligands (1.4%) were confirmed to strongly inhibit (>75%) the binding of fluorescent labelled FLT3 ligand (FL cytokine) to FLT3 overexpressed in HEK-293 cells, at two different concentrations (5 and 20 μM). Concentration-response curves, obtained for 111 lead-like molecules, confirmed the unexpected tolerance of the FLT3 extracellular domain for low molecular weight druggable inhibitors exhibiting submicromolar potencies, chemical diversity, and promising pharmacokinetic properties. Further investigation of one hit confirmed inhibitory properties in dorsal root ganglia neurons and in a mouse model of neuropathic pain.

INTRODUCTION

Receptor tyrosine kinases (RTKs) constitute a subset of 58 membrane-spanning kinases involved in key cellular processes such as growth, survival, and differentiation.[1] They share a conserved structural architecture consisting in an extracellular ligand-binding domain, a single transmembrane helix, and an intracellular kinase domain exhibiting a catalytic phosphorylation activity.[2] Upon binding of endogenous growth factors and cytokines to the extracellular domain, RTK undergo first dimerization and then the cross-phosphorylation of intracellular domains, each chain phosphorylating the neighboring chain by its kinase-containing region.[3] Depending on the exact pattern of phosphorylated tyrosines, different effectors (e.g., Src family tyrosine kinases)[4] are recruited thereby initiating a specific intracellular signaling pathway. Since RTK are dysregulated in a wide array of pathologies ranging from cancer[5] to neurological diseases,[6] they have attracted considerable attention from the pharmaceutical industry to design molecular strategies aiming at blocking their catalytic activity. Among the many ways to block RTK-mediated cell signaling[5] (**Figure 1A**), the most popular strategy has been to block the catalytic activity of the kinase domain by ATP-competitive inhibitors (e.g., sunitinib),[7] leading notably to spectacular progresses in cancer chemotherapy.[8] However, the conserved architecture of the ATP catalytic site throughout the kinome, usually hampers the fine selectivity of kinase inhibitors, thereby often leading to multiple kinases inhibition and undesirable side effects[9-10] that may be acceptable in cancer therapy but not for non-life-threatening chronic diseases. Exquisite selectivity can only be achieved by monoclonal antibodies targeting either the ligand (e.g., bevacizumab)[11] or the RTK extracellular domain (e.g., trastuzumab),[12] thus preventing the recognition of the endogenous growth factor and consequently RTK activation. Because of their high production costs, monoclonal antibody therapies remains very expensive (ca. 100,000 USD per year).[13] Low molecular weight inhibitors would therefore be highly desirable to achieve a comparable extracellular inhibition. RTK modulation by small molecules at the extracellular level has rarely been described (**Figure 1B**), despite obvious advantages among which selectivity, safety and possibly pathway-biased signaling.[14] To the best of our knowledge, we reported the first-ever described RTK negative allosteric

modulator (NAM), ANA-12 (**Figure 1B**), a high-affinity NAM of the neuronal TrkB receptor which prevents in a non-competitive manner BNDF binding to the extracellular d1-d5 domain of TrkB, and exhibits potent anxiolytic and antidepressant properties in rodents.[15] A couple of years later, Bono et al reported the discovery of SSR128129E, a non-competitive inhibitor of FGFR receptor subtypes.[16] Strinkingly, the compound is much more potent in inhibiting FGF2-induced cellular responses (IC_{50} in the 10-30 nM range) than inhibiting FGF2 binding *in vitro* (IC_{50} = 1.9 µM), a discrepancy explained by the specific environment of endothelial cells and conformational properties of intact FGFR. Nuclear magnetic resonance spectroscopy unambiguously demonstrated direct binding of the inhibitor to the d3 domain of FGFR3[17] at a site distant from that of FGF ligands. Oral administration of the compound blocks angiogenesis and growth of tumors refractory to anti-vascular endothelial growth factor receptor-2 antibodies.

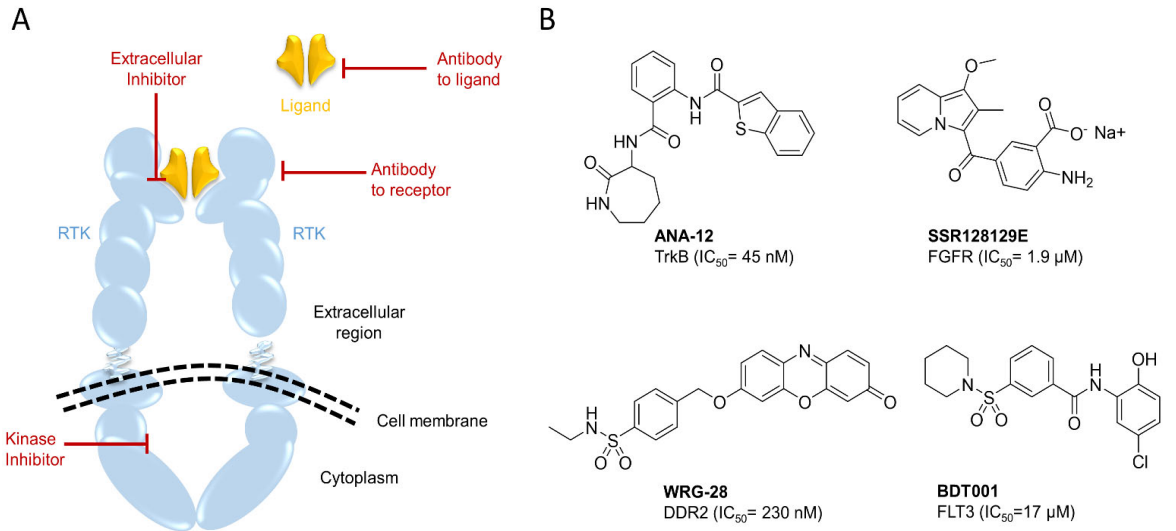

Figure 1. RTK structure and allosteric modulation (**A**) Possible molecular strategies leading to RTK inhibition; (**B**) Structure of known RTK allosteric modulators

Along the same line, WRG-28 was recently described as an extracellular allosteric inhibitor of DDR2, the collagen-binding receptor tyrosine kinase.[18] The compound inhibits DDR2 signaling in vivo and significantly reduces metastatic lung colonization of breast tumor cells in mice.

Last, we recently reported BDT001 as a micromolar NAM of the FLT3 receptor.[19] Similarly to the above-described FGFR inhibitor, the compound is much more potent (IC_{50} = 150 nM) in inhibiting FLT3 ligand-induced calcium responses to TRPV1 activation in dorsal root ganglion (DRG) neurons, than to block FLT3 ligand binding to FLT3-overexpressing HEK cells. Furthermore, BDT001 exhibits potent and long-lasting anti-hyperalgesic and anti-allodynic properties in rodents. Since FLT3 is believed to be the main trigger of peripheral neuropathic pain,[19] FLT3 allosteric inhibitors open a novel avenue to the first specific treatment of neuropathic pain, a chronic disease state for which repurposed anti-epileptics (e.g. pregabalin)[20] and anti-depressants (e.g., amitriptyline)[21] have been the main symptomatic treatment albeit with poor efficacies and significant side-effects.[22] Unfortunately, BDT001 is not directly developable for human use because of fast metabolic degradation and drug-drug interaction liabilities.[19] Identifying alternative chemotypes with better pharmacokinetic (PK) properties would therefore be highly desirable. Herein, we report the high-throughput screening of the French Chemical Library (48,000 compounds) using an *in vitro* time-resolved fluorescence energy transfer (TR-FRET) assay. We further describe the hit selection and validation process leading to eight chemically different low molecular weight FLT3 inhibitors with promising early PK profiles, one of which demonstrated FL antagonism in DRG neurons and pain relief in a mouse model of neuropathic pain.

RESULTS AND DISCUSSION

Development of an automated and miniaturized in vitro binding assay. To discover novel FLT3 inhibitors, we developed a homogeneous time-resolved fluorescence (HTRF) competition assay, based on the fluorescence energy transfer (FRET) between a donor and an acceptor fluorophore.[23] HEK-293 cells overexpressing the FLT3 receptor labeled with Lumi4-Tb-donor-derivatized benzylguanine substrate (SNAP-Lumi4-Tb) were first seeded into 384-well plates. Then compounds (or controls) were added into the wells. The FL-d2 ligand (FLT3-ligand FL labeled with d2) was added one hour later. After 20 h incubation, reading (excitation 337 nm; emission 615 and 665 nm) was performed in a microplate reader. Ratio calculation between 665 and 615 nm fluorescence units allows the identification of compounds that interfere with the TR-FRET measurement in the assay when compared to the control wells (FL-d2 binding to FLT3-Tb). A binding inhibition over 75% was used as a threshold for hit selection. The robustness and quality of the primary screening assay were evaluated by using the Z' factor[24] for every plate. We obtained values over 0.5 which are significant to validate the plates (for assay development and in every plate during the screening).

Primary screening and confirmatory concentration-response curves. The French Chemical Library (FCL)[25] is a screening deck of ca. 70,000 compounds including 15,000 natural product extracts, originating from 45 French academic laboratories and available for screening as 96 or 384-well plates at the concentration of 5 mM in DMSO. 48,320 FCL compounds were here screened according to a multi-step flowchart (**Figure 2**).

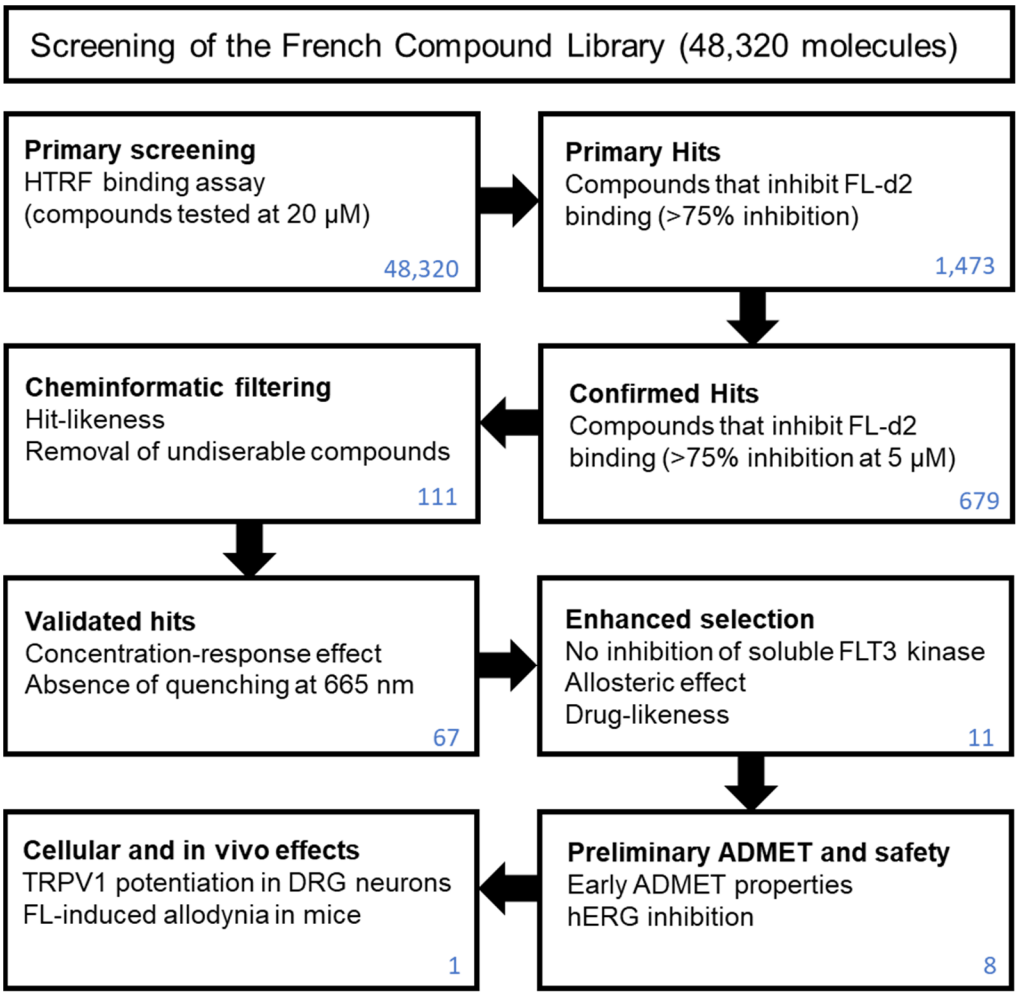

Figure 2. Screening flowchart of the French Compound Library to identify negative allosteric modulators of the FLT3 receptor tyrosine kinase. Numbers in blue indicate the number of compounds selected at each stage.

First, all compounds were tested, using the above-described HTRF assay, at the single concentration of 20 µM for their capacity to inhibit the binding of the fluorescent labelled FL-d2 cytokine to Lumi4-Tb-SNAP-FLT3 overexpressed in HEK-293 cells. Surprisingly, the primary screen returned a wide array of potential hits (n=1,473) that diminished by more than 75% the ratio between 665 and 615 nm fluorescence signals (**Figure 3**).

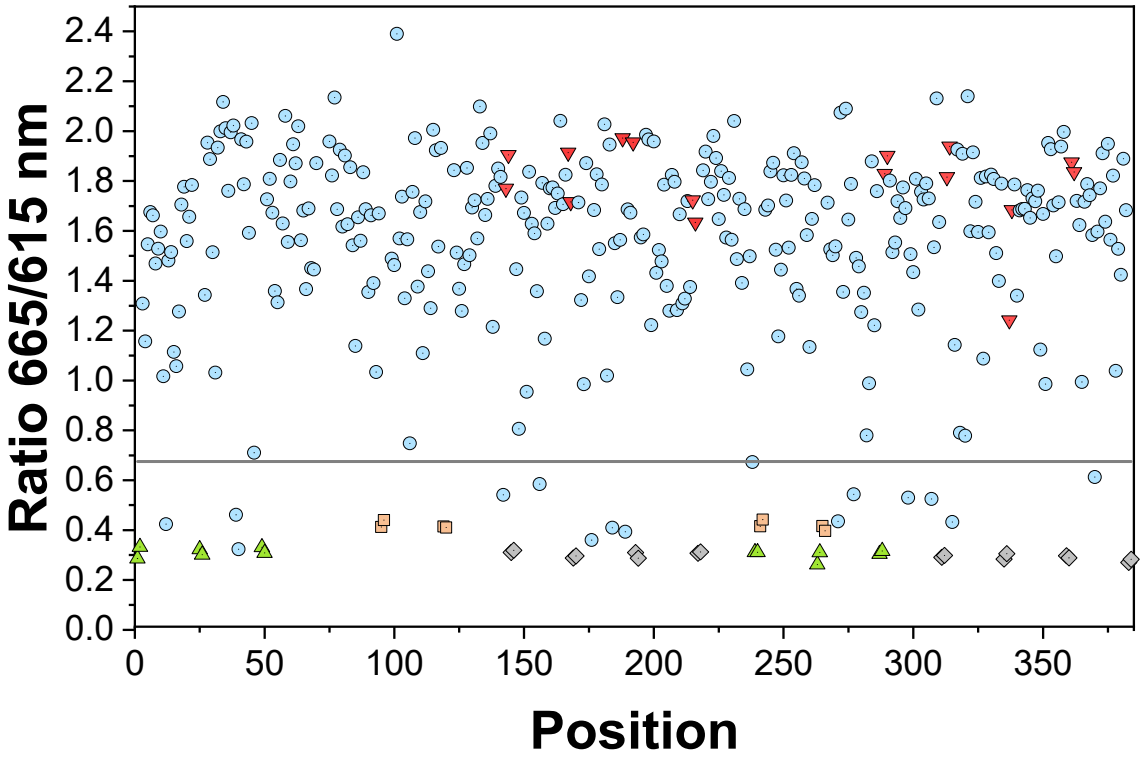

Figure 3: Inhibition of 0.5 nM FL-d2 binding to Lumi4-Tb-SNAP FLT3 overexpressed in HEK-293 cells (8 000 cells/well) monitored by HTRF, as the ratio of fluorescence intensities measured at 665 and 615 nm, on one (out of 151) 384-microtiter plates of the French Chemical Library (FCL). Data are colored as follows: red triangles, 0.5 nM FL-d2 control; green triangles, 0.5 nM FL-d2 + 0.1 µM FL; orange squares, 0.5 nM FL-d2 + 20 µM BDT121 competitor;[26] gray diamonds, buffer only (TBX 1% DMSO); blue circles, 0.5 nM FL-d2 + 20 µM FCL competitor). Plate positions are numbered horizontally from 1 (A1 well) to 384 (P24 well). The solid gray line represents a fluorescence ratio corresponding to the threshold (75% inhibition of FL-d2 binding) used to qualify a primary hit.

These primary hits were cherry-picked from the entire FCL collection, plated in 384-well plates at two different concentrations (5 and 20 µM) and tested again using the same HTRF assay. 1,335 hits (92%) could be confirmed for reduction of the 665/615 nm fluorescence ratio by more than 75%, out of which 679 compounds still diminished this ratio by more than 75% at the lower concentration of 5 µM. A cheminformatics analysis permitted to remove potential false positives (e.g. unsuitable

physicochemical properties, potential aggregators, chemically reactive groups) according to a rule-based filter (**Supporting Table S1**) leading to a final set of 111 hits. These 111 compounds were cherry-picked again and plated in 384-well plates at 10 concentrations (from 1.58 nM to 50 µM) for establishing full concentration-response curves, still using the above-described HTRF binding assay. For 67 out of the 111 compounds (**Figure 4**), concentration-response curves could be obtained (e.g. **Supporting Figure S1A**) with half-maximal inhibiting concentration (IC_{50}) ranging from 33 µM to 10 nM (**Table 1**). The remaining 44 molecules were discarded because of either a too low FRET signal at the lowest concentration (e.g., **Supporting Figure S1B**), a concentration-independent low FRET signal (e.g., **Supporting Figure S1C**), or quenching the 665 nm fluorescence. Altogether, the 67 remaining compounds could therefore be considered as true inhibitors of FL binding and selected as validated hits. The hit rate calculated with these 67 validated hits was 0.14%, which is within the hit rate range for high throughput screenings.

Class 1: 6H-pyrido[4,3-b]carbazoles and analogues

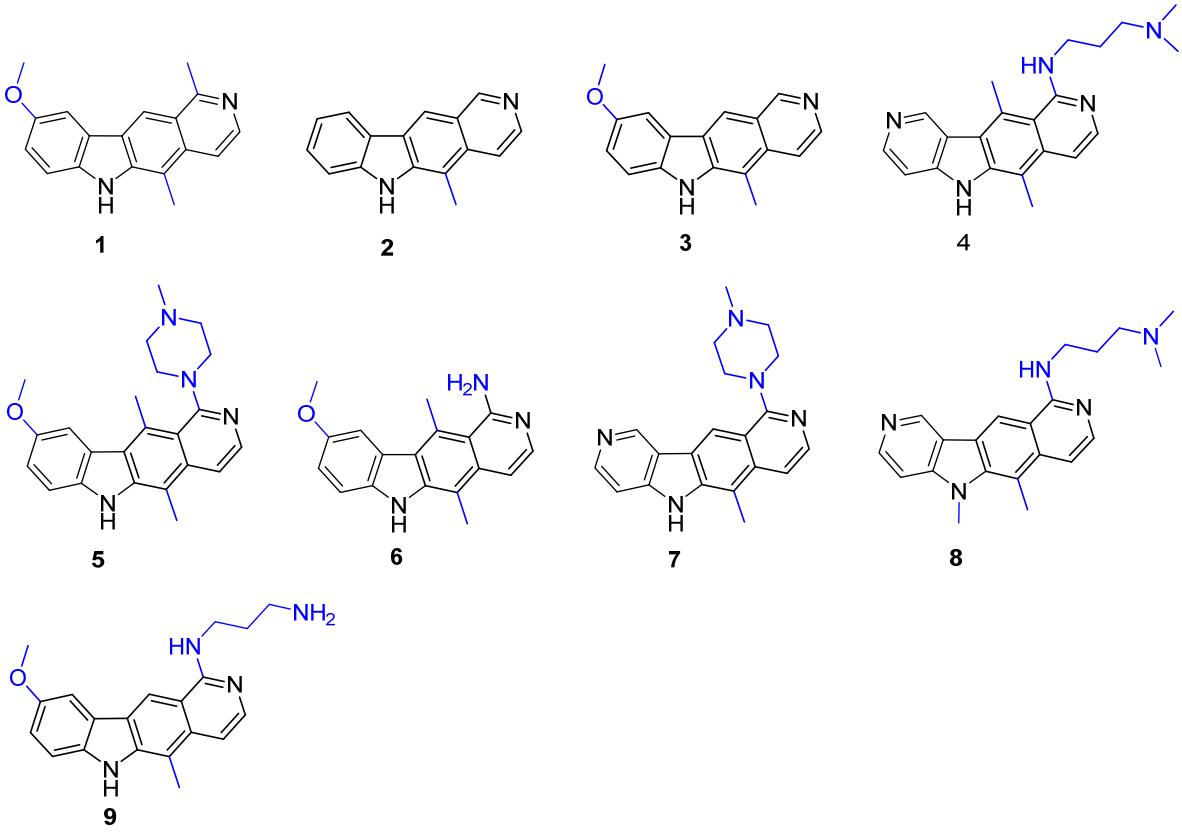

Class 2: 5H-pyrido[4,3-b]indoles and analogues

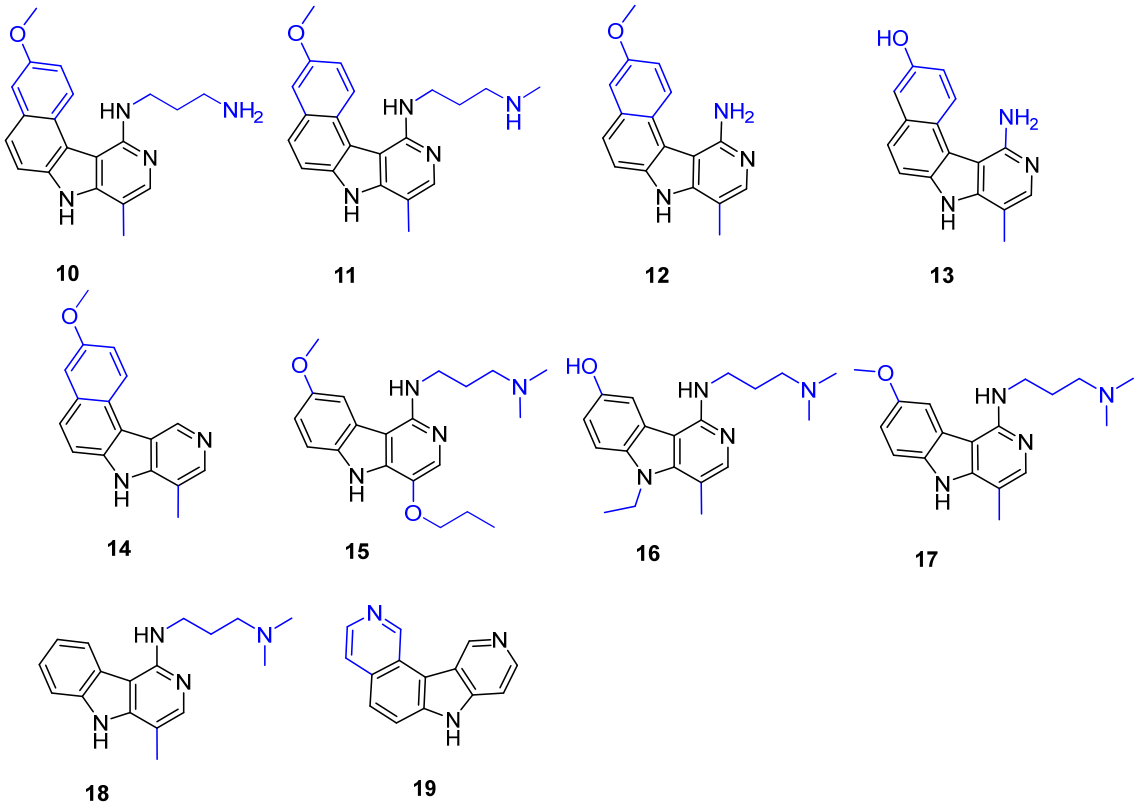

Class 3: 2H-chromen-2-ones and analogues

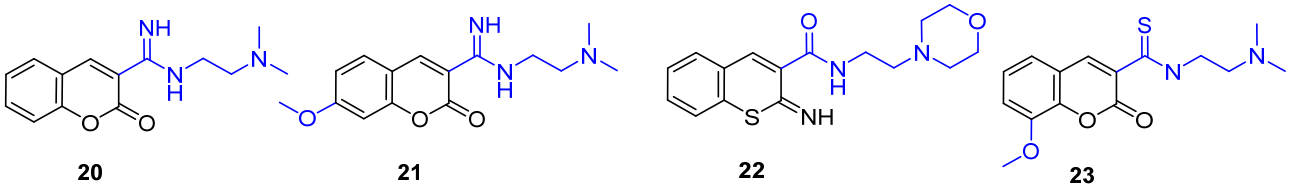

20 **21** **22** **23**

Class 4: 11λ^3-benzo[c]phenanthridine sand analogues

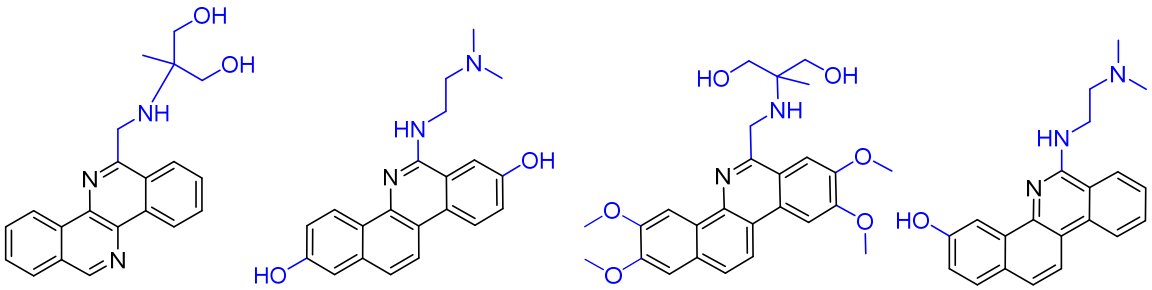

24 **25** **26** **27**

Class 5: pyrrolo[1,2-a]quinoxalines and analogues

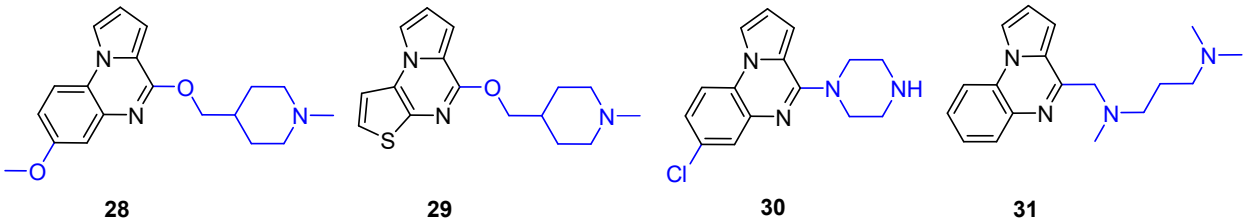

28 **29** **30** **31**

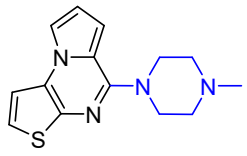

32

Class6: benzo[h]quinolines and analogues

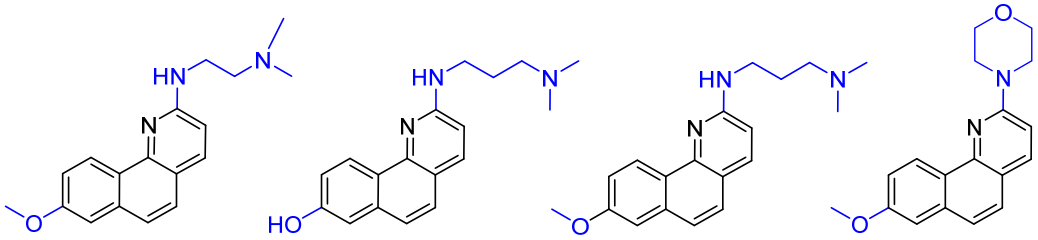

33 **34** **35** **36**

Class 7: 7H-pyrido[3,4-c]carbazoles and analogues

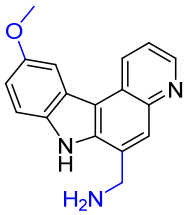

37

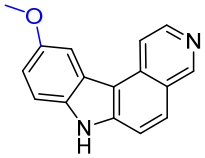

38

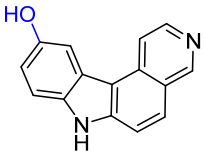

39

Class 8: Isoquinolines and analogues

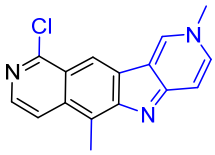

40

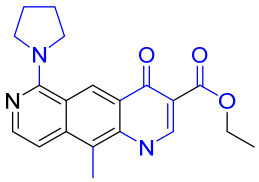

41

Class 9: N-(5,6-dihydro-4H-cyclopenta[c]thiophen-4-yl)-2-(piperazin-1-yl)acetamides and analogues

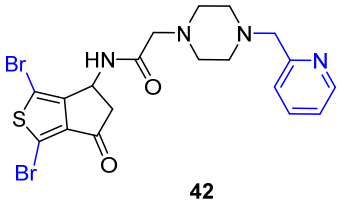

42

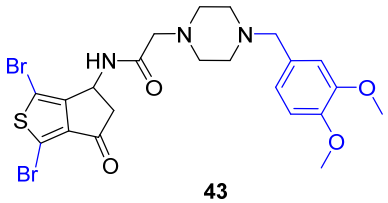

43

Class 10: 6-phenyl-pyridazines and analogues

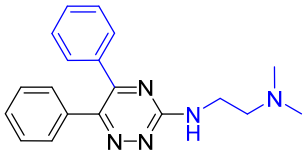

44

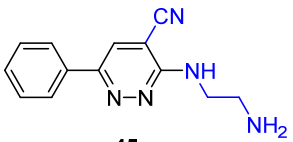

45

Class 11: benzo[b][1,6]naphthyridines and analogues

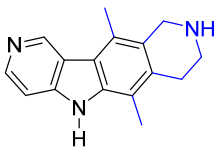

46

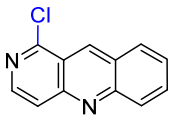

47

Singletons:

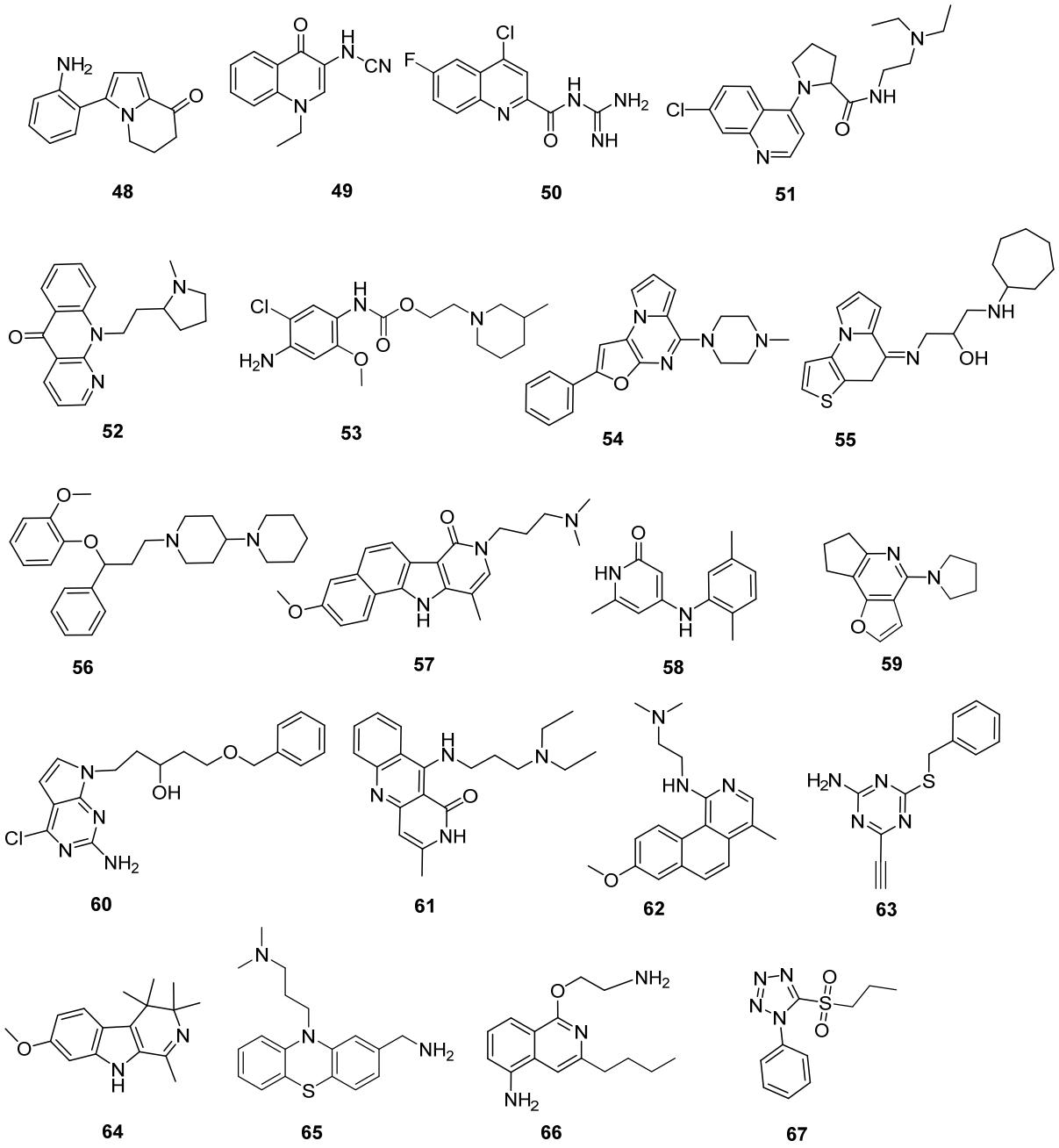

Figure 4. Chemical structure of 67 validated hits. The chemical scaffold representative of each class is displayed in black, and the substituents in blue. Singletons correspond to compounds that cannot be clustered with any other hit.

Table 1. Binding inhibition of 67 validated hits at the FLT3 receptor tyrosine kinase.

Cpd	IC_{50}, µM[a]	Ligand efficiency[b]	Cpd	IC_{50}, µM	Ligand efficiency
1	2.53 ± 0.48	0.36	**35**	0.21 ± 0.03	0.40
2	33.62 ± 6.59	0.34	**36**	0.10 ± 0.02	0.43
3	1.14 ± 0.16	0.41	**37**	1.06 ± 0.08	0.39
4	0.22 ± 0.02	0.35	**38**	1.89 ± 0.32	0.41
5	0.03 ± 0.005	0.37	**39**	2.74 ± 0.56	0.42
6	0.22 ± 0.03	0.41	**40**	1.06 ± 0.24	0.41
7	0.01 ± 0.002	0.44	**41**	0.17 ± 0.04	0.35
8	0.07 ± 0.01	0.38	**42**	1.18 ± 0.23	0.29
9	0.58 ± 0.09	0.34	**43**	0.29 ± 0.07	0.28
10	0.52 ± 0.08	0.34	**44**	0.46 ± 0.07	0.36
11	0.36 ± 0.04	0.34	**45**	0.84 ± 0.16	0.46
12	0.09 ± 0.02	0.46	**46**	0.15 ± 0.01	0.49
13	1.21 ± 0.33	0.40	**47**	3.58 ± 0.53	0.50
14	0.12 ± 0.02	0.47	**48**	0.71 ± 0.17	0.49
15	0.17 ± 0.03	0.35	**49**	0.85 ± 0.16	0.52
16	0.66 ± 0.8	0.35	**50**	2.14 ± 0.39	0.43
17	0.42 ± 0.5	0.38	**51**	0.60 ± 0.14	0.34
18	0.65 ± 0.11	0.40	**52**	0.99 ± 0.20	0.37
19	0.27 ± 0.04	0.53	**53**	0.51 ± 0.10	0.36
20	0.45 ± 0.07	0.46	**54**	0.26 ± 0.04	0.34
21	0.22 ± 0.04	0.43	**55**	0.40 ± 0.07	0.36
22	0.03 ± 0.005	0.47	**56**	0.38 ± 0.07	0.29
23	0.10 ± 0.02	0.45	**57**	0.08 ± 0.01	0.32
24	0.52 ± 0.07	0.33	**58**	0.33 ± 0.05	0.52
25	0.12 ± 0.01	0.36	**59**	0.33 ± 0.03	0.52
26	0.19 ± 0.03	0.27	**60**	7.25 ± 1.85	0.28
27	0.04 ± 0.005	0.40	**61**	0.07 ± 0.02	0.39
28	0.21 ± 0.04	0.38	**62**	0.13 ± 0.03	0.41
29	0.52 ± 0.06	0.41	**63**	0.94 ± 0.14	0.48
30	0.14 ± 0.03	0.47	**64**	0.47 ± 0.09	0.43
31	0.06 ± 0.005	0.45	**65**	0.07 ± 0.01	0.44
32	0.48 ± 0.12	0.45	**66**	0.16 ± 0.04	0.44
33	0.41 ± 0.5	0.40	**67**	1.22 ± 0.22	0.47
34	0.23 ± 0.04	0.41			

[a] Binding constants are derived from dose-response curves of FCL competitors in inhibiting the binding of fluorescent-labelled FL-d2 to Lumi4-Tb-SNAP-FLT3 overexpressed in HEK-293 cells. The ratio of fluorescence intensities emitted at 665 and 615 nm (indicative of FL-d2 binding and subsequent FRET signal) is measured at 10 concentrations of the competitor in triplicate. Half-maximal inhibiting concentration (IC_{50}) is given as mean ± SEM.

[b] Ligand efficiency[27] = $-RT\ln(IC_{50})/HAC$ (HAC: heavy atoms count), T=298K

Chemical diversity of validated hits. The 67 validated hits were clustered in 11 chemical classes according to their maximum common substructures (**Figure 4**). 20 molecules were defined as singletons and could not be attributed to any of the 11 classes. Many classes are described by either tetracylic (classes 1, 2, 4, 7, 8 and 12) or tryclic (class 6) heteroaromatic systems bearing protonated amine 3 to 4 atoms away from the aromatic polycyclic structure. However, a great scaffold diversity can be found, notably among the 20 singletons. Interestingly, 54 out of the 67 hits present IC_{50} values below 1 µM (**Figure 5A**), a rather surprising result owing to the presumed low druggability of the FLT3 extracellular domain. Since the molecular weight distribution is centered on the rather low value of 300 Da (**Figure 5C**), many hits exhibit excellent ligand efficiency values[27] (**Table 1**, **Figure 5B**) well above 0.40 kcal.mol^{-1} per heavy atom. Therefore, the selected hits constitute potential interesting starting points for hit to lead optimization. Calculating standard molecular properties (e.g., AlogP, H-bond acceptor and donor counts, number of rotatable bonds and rings) further evidences the lead-like properties of most compounds (**Figure 5C-H**) that all are Lipinski's rule-of-5[28] compliant.

Final hit selection. All above-reported hits might not be developable for many reasons among which low ligand efficiency, known or potential off-target/ADMET liabilities, and intracellular FLT3 kinase inhibition. A key asset of the FCL deck is that compounds can be traced back at laboratories which originally synthetized them, and annotated by pharmacological properties. We therefore discarded 47 validated hits for two major reasons. Firstly, 37 compounds (**1**-**19**, **24**-**27**, **33**-**41**, **46**-**47**, **61**-**62**, **64**) are ellipticine analogs with known or potential DNA-intercalating properties and are probably not developable for treating chronic pain. Secondly, 10 compounds were not further considered because of low ligand efficiency values (**42**, **43**, **51**-**57**, **60**; **Table 1**) and high molecular weight, which could make a hit to lead optimization program more difficult.

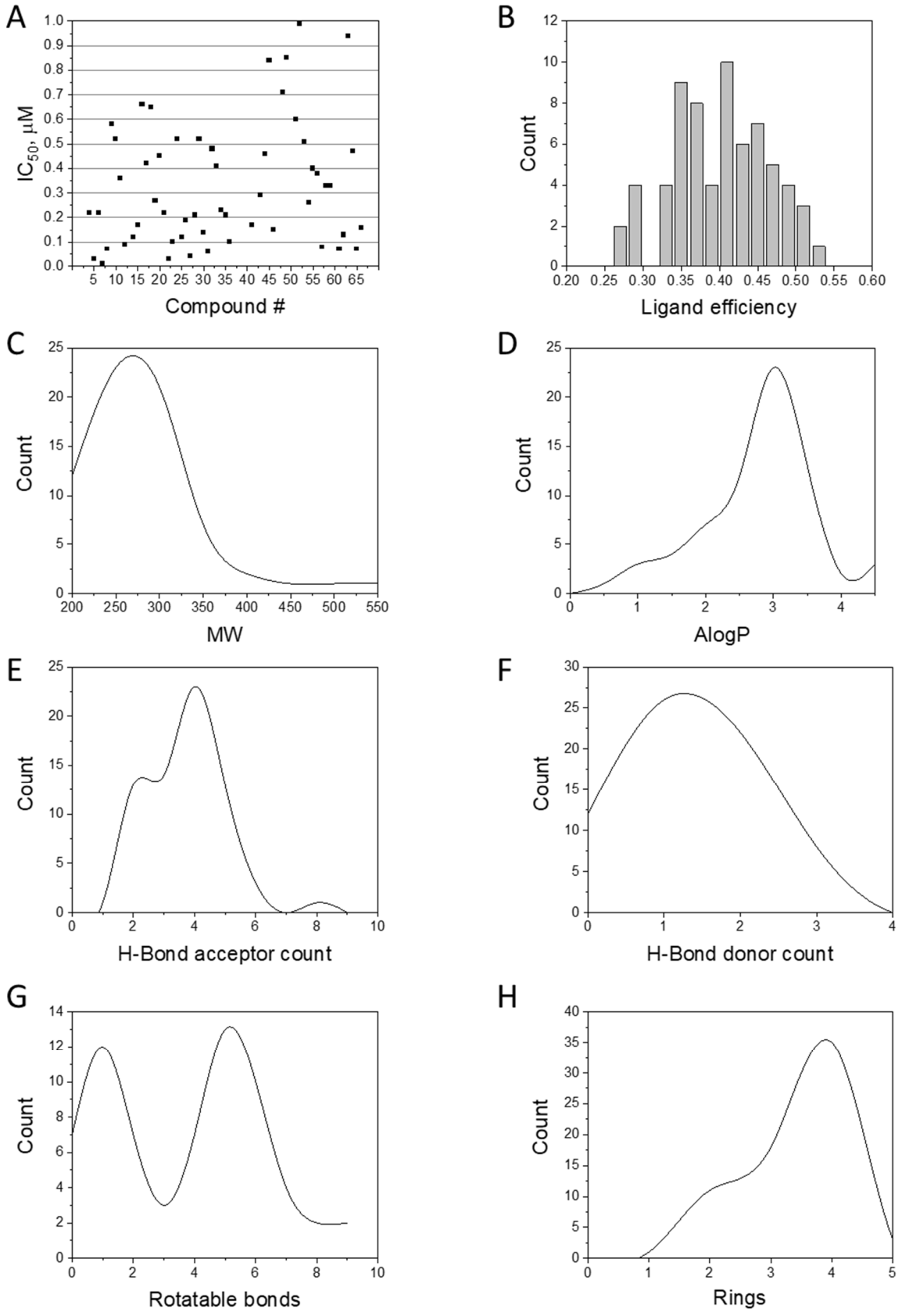

Figure 5. Properties of the 67 validated hits. **A)** Distribution of IC_{50} values (excluding 7 compounds with IC_{50} > 1µM), **B)** Ligand efficiency, **C)** Molecular weight, **D)** AlogP, **E)** H-bond acceptor count, **F)** H-bond donor count, **G)** Number of rotatable bonds, **H)** Number of rings.

Table 2. Non-competitive inhibition of representative hits at two different FL-d2 concentrations

Cpd	IC_{50}, µM 0.5 nM Fl-d2	IC_{50}, µM 2 nM FL-d2
7	0.14 ± 0.01	0.22 ± 0.02
22	0.06 ± 0.005	0.13 ± 0.01
23	0.23 ± 0.01	0.22 ± 0.02
28	0.25 ± 0.02	0.32 ± 0.03
44	0.76 ± 0.08	0.92 ± 0.10
48	1.32 ± 0.18	1.60 ± 0.20
49	0.49 ± 0.05	0.68 ± 0.10
59	108.6 ± 19.5	196.0 ± 51.7
65	0.06 ± 0.005	0.08 ± 0.01
66	0.94 ± 0.14	1.26 ± 0.16
67	1.26 ± 0.16	1.79 ± 0.25
Sunitinib	0.06 ± 0.005	0.09 ± 0.01

[a] IC_{5O} values are derived from dose-response curves of FCL competitors in inhibiting the binding of fluorescent-labelled FL-d2 to Lumi4-Tb-SNAP FLT3 overexpressed in HEK-293 cells. The ratio of fluorescence intensities emitted at 665 and 615 nm (indicative of FL-d2 binding and subsequent FRET signal) is measured at 10 concentrations of the competitor in triplicate. Half-maximal inhibitory concentration (IC_{50}) are given as mean ± SEM.

Four hits which are representative of the remaining classes (**22**-**23**, **28**, **44**) and six singletons (**48**, **49**, **59**, **65**-**67**; **Table 2**) were next evaluated from powders of pure compounds (**Supporting Table S2**) on two counter screens. Although ellipticine derivatives have previously been discarded, we kept compound **7** as a representative since many analogs were present among the primary hits. First, non-competitive FLT3 inhibition could be easily evaluated using the same HTRF binding assay, but at two concentrations (0.5 and 2 nM) of fluorescent labeled FL-d2 ligand. The half-maximum inhibitory concentration (IC_{50}) of all tested compounds is independent on the FL-d2 ligand concentration (**Table 2**), thereby evidencing a non-competitive inhibition mechanism of all newly discovered FLT3 inhibitors. Second, soluble FLT3 kinase inhibition had to be investigated because sunitinib, a known intracellular ATP-competitive FLT3 inhibitor (IC_{50} = 9.9 nM)[29] is still able to potently inhibit extracellular FL binding to full-length FLT3 in our HTRF assay (IC_{50}= 64 nM; **Table 1**; **Supporting Figure 2**). Inhibition of the soluble FLT3 kinase was measured for 11 representative hits (**Table 2**) by a functional luminescent assay measuring ATP to ADP conversion, and demonstrated that all hits but compound **7** did not inhibit the catalytic activity of the soluble FLT3 kinase (**Figure 6**). Since compound **7** is structurally related to

33 hits from 7 chemical classes (1, 2, 4, 6, 7, 8 and 12) it is likely that the latter compounds are also intracellular inhibitors of the kinase domain. This observation probably explains the unexpected high hit rate previously observed in the primary screening assay because the HTRF assay cannot discriminate genuine extracellular NAMs from all classical ATP-competitive kinase inhibitors present in the FCL repository. The exact mechanism by which intracellular inhibitors may block at a very large distance, the binding of FL to the extracellular FL3 domain (**Figure 1**) remains unknown. Recent biostructural studies clearly evidence that ligand binding to RTK clearly induces subtle conformational changes at either the extra- or the intracellular domain, inducing a modification of the equilibrium between monomeric and dimeric states, as well as ligand-specific microstates of the intracellular domain inducing selective phosphorylation patterns.[30] Stabilization of the intracellular domain by sunitinib probably induces a peculiar conformation of the extracellular domain that is no more competent to bind the FL cytokine.

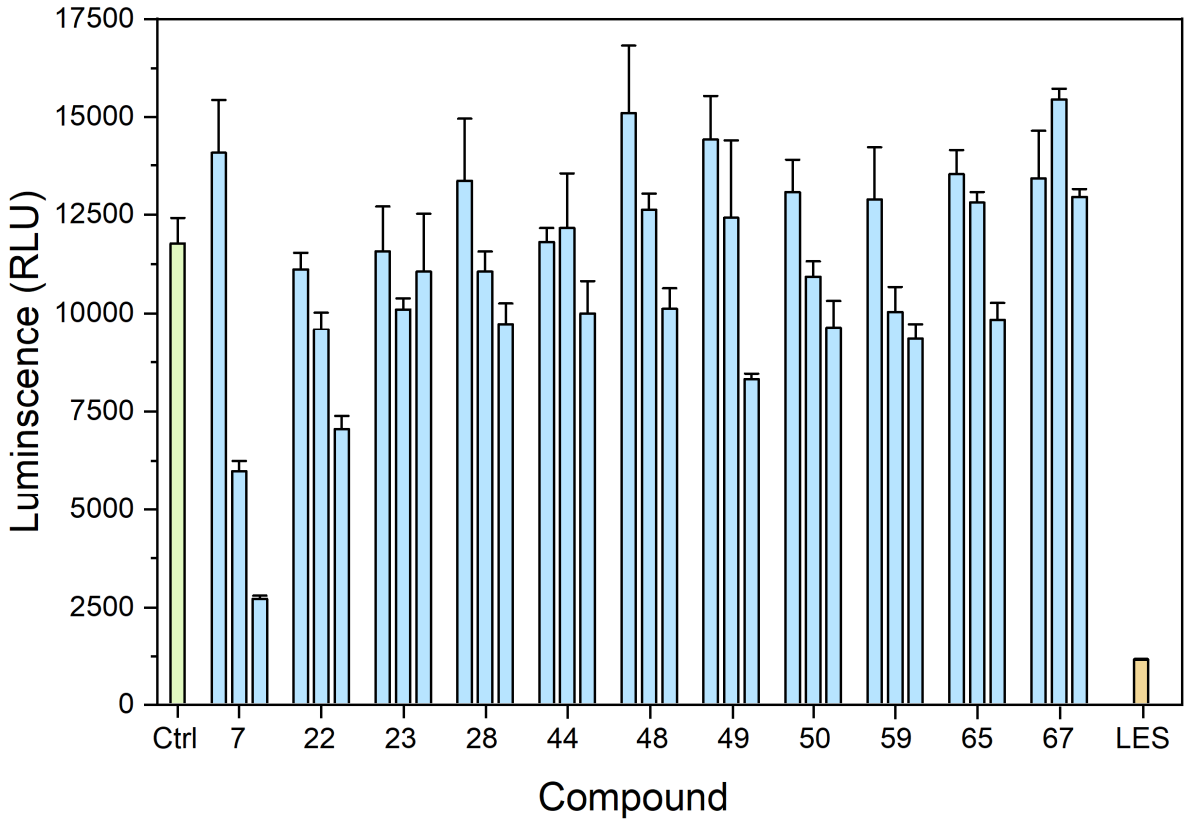

Figure 6. Inhibition of soluble FLT3 kinase by FCL competitors. Each compound is tested at three concentrations (left bar: 0.5 µM, middle bar: 2 µM, right bar: 20 µM) in triplicate by a luminescent assay (Promega ADP-Glo™ kinase Assay) measuring ADP formation from the soluble FLT3 Kinase using a 50 µM ATP concentration (Ctrl, no competitor; LES, 100 µM Lestaurtinib). Luminescence is expressed as relative light units (RLU).

Early ADMET properties of eight representative hits. Eight representative compounds (**22**, **23**, **30**, **44**, **48**, **49**, **65**, and **67**) of true non-competitive extracellular FLT3 inhibitors were further profiled for preliminary ADMET studies. For each compound, we determined the following key properties: aqueous solubilities in different buffers, human liver microsomal stability, cytochrome P450 (CYP) isoforms inhibition, human plasmatic protein binding, Caco-2 cell permeation and hERG channel inhibition (**Table 3**). Several hits display noticeable liabilities and clearly requires a multi-parametric optimization. For example, compounds **30**, **44**, **48,** and **65** exhibit significant CYP and hERG channel inhibitions at a 10 µM concentration, that need to be minored. Compounds **30**, **65** and **67** present a very low permeability of Caco-2 cell monolayers indicative of poor intestinal absorption if given orally, with a strong efflux (B-A >> A-B permeability) for compound **65**. In addition, off-targets and/or biological activities have already been reported for some of the above-mentioned compounds. For example, compound **30** as well as all pyrroloquinoxalines of class 5 are potent agonists of the serotonin 5-HT_3 receptor subtypes.[31] Likewise, compound **44** and its close analog **45** (class 10) were originally developed as acetylcholinesterase inhibitors.[32] Compound **65** is a trypanothione reductase inhibitor with anti-parasitic properties,[33] and compound **66** blocks nicotinic acetylcholine receptors.[34] These observations do not disqualify the above-cited compounds for hit to lead optimization but just indicate lines along which these hits still need improvements. Hit **49** exhibits excellent ADMET properties but bears an electrophilic cyanamide group, known to favor covalent binding to free cysteine-containing enzymes in a reversible manner,[35] that should therefore be removed or replaced without affecting FLT3 binding before any further optimization. Altogether, the thiochromene-2-imine **22**[36] appears as a good compromise for hit to lead development. Despite a high but manageable protein plasmatic protein binding and moderate cytochrome P450 (CYPs) inhibition, compound **22** display overall satisfactory ADMET properties. Interestingly, it is one of the most potent FLT3 inhibitor of our 111 validated hits (**Tables 1, 2**) and is part of class 3 (**Figure 3**), comprising three related analogs exhibiting good potencies in the confirmatory dose-response assay (**Table 1**). Compound **22** was therefore chosen further studies on neuronal FLT3 inhibition and in vivo anti-hyperalgesic property evaluation.

Table 3. Early ADMET properties of eight representative hits

Property	Compound							
	22	**23**	**30**	**44**	**48**	**49**	**65**	**67**
Molecular weight (g/mol)	317.46	306.38	286.76	319.41	252.29	213.24	313.46	212.29
clogP[a]	0.81	1.54	2.57	3.31	2.71	1.67	3.00	1.57
Aqueous solubility (PBS buffer, pH 7.4), µM[b]	n.d.[l]	69.3	142.9	>200	173.9	144.3	152.2	192.5
Aqueous solubility(simulated intestinal fluid), µM[b]	n.d.	82.7	146.4	> 200	159.3	177.8	156.3	167.8
Aqueous solubility(simulated gastric fluid), µM[b]	n.d.	200.0	182.5	> 200	194.4	181.0	200.0	177.1
Human plasmatic protein binding %	99	92	92	78.4	95	86	79	n.d.
Caco-2 permeation, P_{app} A-B, 10^{-6} cm/s	35.43	32.6	3.9	39.8	34.1	14.4	1.3	1.6
Caco-2 permeation, P_{app} B-A, 10^{-6}cm/s	34.49	19.4	2.5	25.2	15.6	32.2	10.2	0.2
Human liver microsome stability, $t_{1/2}$, min.	>60	34.7	> 60	> 60	33.0	> 60	> 60	> 60
Human liver microsome stability, % remaining after 60 min.	56.8	31.8	56.6	87	29.4	56.87	69.1	75.9
CYP1A2 inhibition, %[c]	35.0	68.8	88.8	15.2	48.3	2.9	54.0	8.2
CYP2B6 inhibition, %[d]	47.2	16.9	82.6	13.0	65.7	5.9	59.4	38.9
CYP2C8 inhibition, %[e]	51.5	-9.8	-6.8	13.7	0.6	11.6	18.4	-5.6
CYP2C9 inhibition, %[f]	12.8	2.7	0.2	91.9	16.1	8.9	10.6	6.6
CYP2C19 inhibition, %[g]	51.1	41.0	30.9	31.9	47.8	14.3	35.8	24.2
CYP2D6 inhibition, %[h]	59.3	28.2	52.2	91.9	36.3	18.0	54.8	12.4
CYP3A4 inhibition, %[i]	8.8	3.2	9.4	3.5	37.9	2.9	3.5	15.3
CYP3A4 inhibition, %[j]	15.9	16.2	52.5	32.1	32.8	17.0	10.8	14.4
hERG inhibition, %[k]	24.2	13.1	86.4	42.5	72.7	49.9	80.3	10.7

[a]Computed with ChemAxon MarvinSketch (consensus method). [b]Kinetic solubility measured by HPLC-UV/VIS. [c]Inhibition of CYP1A (phenacetin substrate) at 10 µM. [d]Inhibition of CYP2B6 (bupropion substrate) at 10 µM. [e]Inhibition of CYP2C8 (amodiaquine substrate) at 10µM. [f]Inhibition of CYP2C9 (diclofenac substrate) at 10 µM. [g]Inhibition of CYP2C19 (omeprazole substrate) at 10 µM. [h]Inhibition of CYP2D6 (dextromethorphan substrate) at 10 µM. [i]Inhibition of CYP3A (midazolam substrate) at 10µM. [j]Inhibition of CYP3A4 (testosterone substrate) at 10 µM. [k] Inhibition of [^{3}H-dofetilide] binding, [l] Not detected by the analytical method (UV-VIS). The test compound may not have a sufficient chromophore or may elute outside the window of the default gradient method.

Inhibition of neuronal FLT3 alleviates FL-induced TRPV1 potentiation and mechanical allodynia in mice. We have already shown that the FL cytokine potentiates capsaicin-evoked activation of the TRPV1 ion channel, thereby provoking a massive entry of calcium ions in DRG neurons, which is a hallmark of peripheral neuronal hyperexcitability observed in neuropathic pain.[19] As previously observed with our prototypical FLT3 inhibitor BDT001 (**Figure 1**), compound **22** also inhibits the FL-induced TRPV1 activation in DRG neurons *in vitro* with a complete inhibition of FL effects at the concentration of 0.1 µM (**Figure 7A**).

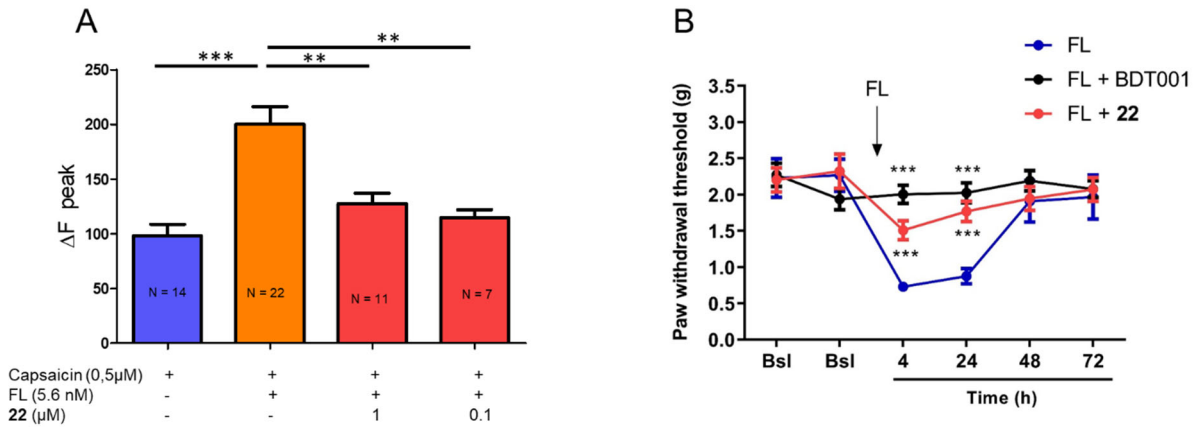

Figure 7. Inhibition of FL-induced responses in mice DRG neurons. **A)** Inhibition of FL-induced TRPV1 potentiation in DRG neurons in vitro. Compound **22** (1 and 0.1 µM) inhibited potentiation by FL (5.6 nM) of capsaicin-induced increases in $[Ca^{2+}]_i$ levels in sensory DRG neurons in vitro. Results are means ± SEM of data obtained from the number of neurons indicated in columns. *P < 0.05; **P < 0.01; ***P <0.001 by one-way ANOVA followed by Bonferroni's multiple comparison test. **B)** Inhibition of FL-induced pain allodynia in mice. BDT001 (5 mg/kg i.p.) and compound **22** (5 mg/kg i.p.) inhibited punctuate tactile stimuli induced by FL (50 ng/5µl, injected intrathecally) as measured by the Von Frey filament test (up and down method). Mechanical allodynia was measured 4, 24, 48 or 72 h after injection. Bsl, basal scores before FL injection. Results are means ± SEM of data from 8 animals. *P < 0.05; **P <0.01; ***P < 0.001 vs. FL-vehicle by two-way ANOVA with repeated measures and Bonferroni's comparison test.

The anti-hyperalgesic properties of compound **22** were next evaluated *in vivo*, in the FL-induced hyperalgesia model,[19] used here as a proxy to more invasive neuropathic pain models (e.g., chronic constriction injury, spare nerve ligation)[37] because anti-hyperalgesic and anti-allodynic effects of our lead compound BDT001 were remarkably similar in these three assays.[19]

Intraperitoneal administration of compound **22** to mice at the dose of 5 mg/kg alleviates FL-induced mechanical allodynia in the standard Von Frey filament test,[38] with a partial effect after 4 h and an almost complete reversal of allodynia after 24 h, similarly to the reference BDT001 inhibitor (**Figure 7B**). Noteworthy, the duration of the anti-allodynic effect observed in vivo seems independent on the *in vitro* FLT3 inhibitory potency and pharmacokinetic properties of the inhibitor. While compound **22** is a potent (IC_{50} = 60 nM, **Table** 2) and metabolically stable (at least against mouse liver microsomes, **Table 3**) FLT3 inhibitor, BDT001 is much less potent in vitro (IC_{50} = 17 μM) and quickly degraded after less than 10 min.[19] but displays a comparable efficacy in this *in vivo* model. The FLT3 inhibitor-independent long-lasting effect is probably attributable to the time required to restore a complete neuropathic state once the inhibitor has disappeared from the plasma, notably for achieving a complete FLT3 rephosphorylation and a full biosynthesis of nerve injury-induced pain mediators (e.g. ATF3, NPY, TRPV1, TRPA1)[19] in the DRG.

CONCLUSIONS

We herein describe the high-throughput screening of an academic compound library to disclose novel negative allosteric modulators of the FLT3 receptor tyrosine kinase. Using a time-resolved FRET assay, a high number of potential hits (1,473) was found in a primary screening, that were almost all confimed in a secondary screening utilizing the same HTRF technology. Stepwise filtering of the hit list to eliminate potential false positives and select the most potent and drug-like compounds afforded a final selection of 67 compounds validated by concentration-response curves. The final validated hit rate after the selecting procedure (0.14%) was within the hit rate range for high throughput screenings. Many of these validated hits presented promising early ADMET properties and are amenable to hit-to-lead optimization. One compound (hit **22**) inhibited FL-induced TRPV1 activation in DRG neurons and fully reversed FL-induced mechanical allodynia after systemic administration to mice at the dose of 5 mg/kg.

The current study confirms the very few studies on extracellular inhibition by small molecular-weight compounds[15-16, 18-19] of a very important target class (RTK) and demonstrates that RTK inhibition is not only achievable by intracellular kinase inhibitors or extracellular antibodies. Interestingly, a wide array of chemotypes were found among the newly discovered FLT3 inhibitors suggesting that this RTK exhibits either a single but permissive allosteric cavity in its extracellular domain or independent binding sites at different locations whose occupation allosterically prohibit the binding of the endogeneous cytokine and further receptor activation. Noteworthy, none of the compounds discovered in the current study competitively blocked FL binding to its receptor confirming the low druggability of the FLT3-FL interface. However, negative allosteric modulation can be obtained for a wide array of small molecules with surprisingly high potencies. Negative allosteric modulation of FLT3 translated well in FL-inhibitory properties observed on a more physiological calcium imaging assay on cultured DRG neurons, as well as in the anti-allodynic properties observed after systemic administration to mice. Extracellular NAMs should therefore be definitely considered as a viable and promising strategy for modulating the activity of FLT3 and other receptor tyrosine kinases.

MATERIAL AND METHODS

Production and labeling of cells overexpressing FLT3 receptor. A previously described protocol[39] was slightly modified as follows. The Tag-lite® technology (Cisbio Bioassays, Codolet, France) was used to produce HEK-293 cells overexpressing the FLT3 receptor labeled with Lumi4-Tb-donor-derivatized benzylguanine substrate (SNAP-Lumi4-Tb). When FLT3-ligand FL labeled with d2 (FL-d2) binds to the receptor, the proximity of both fluorophores allows the TR-FRET to occur. HEK293 cells were maintained in DMEM Glutamax (31966, Invitrogen, Courtaboeuf, France) supplemented with antibiotics (penicillin 100 U/ml, streptomycin 100 µg/ml; 15140-122, Invitrogen), and 10 % heat-inactivated Fetal Bovine Serum (10270-106, Invitrogen). The cells were transfected with 15 µg of pCDNA3.1 SNAP-FLT3, 50 µL of Lipofectamine 2000 (11668-019, Invitrogen) and 8 mL of Opti-MEM (31985, Invitrogen) per Petri dishes and then incubated for 24 h at 37°C under 5% CO2. The medium was removed, and 100 nM SNAP-Lumi4-Tb (SSNPTBX, Cisbio Bioassays) diluted in Tag-Lite Buffer (LABMED, Cisbio Bioassays) was added in Petri dishes and then incubated for 2 h at 37°C. Cells were dissociated with trypsin-EDTA (25200-056, Invitrogen), centrifuged during 5 min at 1300 rpm and then washed 3 times with 40 mL of Tag-Lite Buffer. Finally, the labeled cells, suspended in a freezing medium containing 10% of DMSO, were aliquoted and incubated at -80°C overnight in cryo-freezing container before transferring to liquid nitrogen for long-term storage.

Homogeneous time-resolved fluorescence binding assay. All experiments and dilutions were carried out in Tag-Lite Buffer (LABMED, Cisbio Bioassays). HEK-293 cells overexpressing the FLT3 receptor labeled with Lumi4-Tb were thawed, resuspended in Tag-Lite Buffer, and seeded (10 µL/well; 8000 cells/well) in 384-well HiBase PS microplate (784075, Greiner Bio-one) with the Multidrop™ dispenser (Thermo Scientific). The French Chemical Library, delivered as ready-to-use 384-well plates containing 300 nL at 5 mM per well, was diluted by adding 18.5 µL of Tag-Lite Buffer using the robotic pipetting chain (Biomek FXP, Beckman Coulter). Then, 5 µL/well (20 µM) of diluted compounds were added to

the cells and the plates were incubated for 1 h at room temperature before adding 5 µL/well (0.5 nM) of FLT3-ligand FL labeled with d2 (64CUSDAZE, Cisbio Bioassays). The TR-FRET signal was read after 20 h incubation at room temperature with a HTRF-compatible reader (Envision, Perkin Elmer) allowing a donor excitation at 337 nm and a signal collection both at 615 nm and 665 nm (20 flashes, delay 50 µs, integration time 400 µs).

Then HTRF ratio, obtained by dividing the acceptor signal (665 nm) by the donor signal (615 nm), was calculated for each chemical compounds and each control conditions. Z' scores, which estimate the robustness of our assay, were calculated for each plate and were defined as follows:

$$Z' = 1 - \frac{3(SD_{FL} + SD_{FLd2})}{FLd2 - FL}$$

- FLd2 = the mean of HTRF ratio obtained in controls-wells containing FLd2 and cells overexpressing FLT3 receptor;
- FL = the mean of HTRF ratio obtained in controls-wells containing FLd2, cells overexpressing FLT3 receptor and FL- non fluorescent ligand;
- SD_{FL} = standard deviation of HTRF ratio from control-wells containing FLd2, cells overexpressing FLT3 receptor and FL- non fluorescent ligand;
- SD_{FLd2} = standard deviation of HTRF ratio from control-wells containing FLd2 and cells overexpressing FLT3 receptor.

When Z' < 0.5, the plate was invalidated and have been retested in a second time. The threshold for the selection of hit molecules was based on two criteria: (i) the variation of HTRF ratio should be superior to 3-times the standard deviation of the control conditions, and (ii) the inhibition of the FLT3/FLd2 interaction should be superior to 75 %.

Confirmation assay and concentration-response curves. For the confirmation assay, the hits selected in primary screening were tested in duplicate at 5 µM and 20 µM. All the other steps of the protocol and the threshold for the hit selection, remain identical to primary screening. Finally, a dose-response curve from 1.5 nM to 50 µM of each confirmed hits was realized in triplicate. GraphPad Prism 6.01 software (GraphPad Software Inc., San Diego, CA, USA) was used to analyze the data and to determine the IC_{50} ("dose-response inhibition" model).

Chemical clustering. Validated hits were clustered according to their maximum common substructures using the 'Frameworks' method implemented in the MedChem Studio module of the ADMET Predictor v.8.5 package (Simulation Plus Inc., Lancaster, CA 93534, U.S.A.).

Quality control of representative hits. All hits selected for further investigations were checked for identity (high-resolution mass spectrometry) and purity (^{1}H-NMR, LC-MS). All compounds exhibit a purity higher than 95%, except for compound **49** which is found 90.5% pure (**Supporting Table S2**).

2-imino-N-(2-morpholinoethyl)-2H-thiochromene-3-carboxamide (22). Compound was synthesized as previously reported.[36]

^{1}H-NMR (300 MHz, $CDCl_3$) δ 10.31 (s, 1H), 9.10 (s, 1H), 8.48 (s, 1H), 7.54 (dd, *J* = 7.7, 1.5 Hz, 1H), 7.32 (td, *J* = 7.7, 1.5 Hz, 1H), 7.26 – 7.12 (m, 2H), 3.69 – 3.59 (m, 4H), 3.50 (tt, *J* = 6.5, 2.7 Hz, 2H), 2.51 (t, *J* = 6.5 Hz, 2H), 2.47 – 2.40 (m, 4H).

^{13}C-NMR (75 MHz, $CDCl_3$) *δ* 174.1, 163.7, 144.9, 136.7, 133.0, 126.4, 124.4, 123.6, 67.1, 57.1, 53.5, 37.1.

HRMS (ESI) m/z : [M + H]+ Calcd for $C_{16}H_{20}N_3O_2S$ 318.1276; Found 318.1268

Inhibition of soluble FLT3 kinase. The ADP-Glo™ Kinase Assay (#V4064 + V9101) from Promega was used to determine, by a luminescent assay, the quantity of ADP formed from FLT3 kinase reaction, in 384-well small volume plates. More precisely, ADP is converted into ATP, which is converted into light by Ultra-Glo™ Luciferase. Enzyme, substrate, ATP, and compounds are diluted in Tyrosine Kinase Buffer. Briefly, FLT3 kinase (10 ng) was incubated with 50µM of ATP and 0.1µg/µl of MBP Protein in the presence of increasing concentrations of competitors to be tested and incubated for 2 h at room temperature prior to the addition of ADP-Glo™ Reagent for 40 min at room temperature, and of kinase detection reagent for 30 min at room temperature. The luminescent signal was detected using a luminescent microplate reader Plate (Clariostar, BMG Labtech, Ortenberg, Germany). CEP701 (Lestaurtinib), a known intracellular FLT3 kinase inhibitor, was used as a positive control in this assay.

Measurement of preliminary ADMET properties. ADMET properties were determined by Eurofins Discovery (Celle_L'Evescault, France) under the following items: aqueous solubility (item G228), human liver microsome intrinsic clearance (item 607), CYP Inhibition (item G232), human plasma protein binding (2194), bidirectional Caco-2 permeability (item G235), hERG Human Potassium Ion Channel [^{3}H] dofetilide Binding (item 4094)

Adult sensory neuron culture. For calcium imaging, neuron cultures were established from lumbar (L4–L6) dorsal root ganglia.[40] Briefly, ganglia were successively treated by two incubations with collagenase A (1 mg/ml, Roche Diagnostic, France) for 45 min each (37 °C) and trypsin-EDTA (0.25%, Sigma, St Quentin Fallavier, France) for 30 min. They were mechanically dissociated through the tip of a fire-polished Pasteur pipette in neurobasal (Life Technologies, Cergy-Pontoise, France) culture medium supplemented with 10% fetal bovine serum and DNase (50 U/ml, Sigma). Isolated cells were collected by centrifugation and suspended in a neurobasal culture medium supplemented with 2% B27 (Life Technologies), 2 mM glutamine, penicillin/streptomycin (20 U/ml, 0.2 mg/ml) plated at a density

of 2,500 neurons per coverslip and were incubated in a humidified 95% air-5% CO_2 atmosphere at 37 °C.

Calcium imaging. For calcium imaging video microscopy $[Ca^{2+}]i$ fluorescence imaging, DRG neurons were loaded with fluorescent dye 2.5 µM Fura-2 AM (Invitrogen, Carlsbad, CA) for 30 min at 37 °C in standard external solution contained: 145 mM NaCl, 5 mM KCl, 2 mM $CaCl_2$, 2 mM $MgCl_2$, 10 mM HEPES, 10 mM glucose (pH adjusted to 7.4 with NaOH and osmolarity between 300 and 310 mOsm). The coverslips were placed on a stage of Zeiss Axiovert 200 inverted microscope (Zeiss, München). Observations were made at room temperature (20-23°C) with a 20X UApo/340 objective. Fluorescence intensity at 505 nm with excitation at 340nm and 380 nm were captured as digital images (sampling rates of 0.1-2 s). Regions of interest were identified within the soma from which quantitative measurements were made by re-analysis of stored image sequences using MetaFluor Ratio Imaging software. $[Ca^{2+}]i$ was determined by the ratiometric method of Fura-2 fluorescence from calibration of series of buffered Ca^{2+} standards. Neurons were distinguished from non-neuronal cells by applying 25 mM KCl, which induced a rapid increase of $[Ca^{2+}]i$ only in neurons. Pulses of capsaicin were applied at 2 min-intervals and capsaicin and drugs were added after the third pulse. For data analysis, amplitudes of $[Ca^{2+}]i$ increases, ΔF/Fmax, caused by stimulation of neurons with capsaicin were measured by subtracting the 'baseline' F/Fmax (mean for 30 s prior to capsaicin addition) from the peak F/Fmax achieved on exposure to capsaicin. In the absence of any treatment, the distribution of these ratios was well fitted by a normal distribution.

Animals. Experiments were performed in C57BL/6 naive mice (Janvier, France) weighing 25-30 g. All the procedures were approved by the French Ministry of Research (authorization #1006). Animals were maintained in a climate-controlled room on a 12 h light/dark cycle and allowed access to food and water *ad libitum*. Male and female mice were first considered separately in behavioral procedures. Both sexes showed mechanical hypersensitivity of same intensity after intrathecal FL injection (Two-

way ANOVA followed by Bonferroni's test, n = 8 for both sexes). Therefore, experiments were performed only on male mice.

Production of human recombinant FL (rh-FLT3-L). Recombinant FL was produced in the *E. Coli* Rosetta (DE3) strain (Novagen) in our laboratory using the pET15b-rhFL plasmid according to a previously reported protocol.[41] The rh-FL was checked for endotoxin content using the Pyrogen Recombinant Factor C endotoxin detection assay from LONZA (Walkersville MD, USA) and was found free of endotoxins.

Drug delivery. BDT001 (5 mg/kg) or compound **22** (5 mg/kg) were administered intraperitoneally (i.p.). For FL, a 30 G needle attached to a microsyringe was inserted between L4 and L5 vertebrae in lightly restrained, unanaesthetized mice. The reflexive tail flick was used to confirm the punction. A total volume of 5 µl was injected. After intrathecal injection, no mouse presented motor dysfunction, and all the animals were retained for the data analysis.

Punctuate tactile allodynia. Before testing, mice were acclimatized for 60 min in the temperature and light-controlled testing room within a plastic cylinder or on wire mesh. Experimenters were blinded to the drug administered. Tactile withdrawal threshold levels were performed to evaluate mechanical sensitivity and determined in response to probing of the hindpaw with eight calibrated Von Frey filaments (Stoeling, Wood Dale, IL, USA) in logarithmically spaced increments ranging from 0.41 to 15 g (4–150 mN). Filaments were applied perpendicularly to the plantar surface of the paw. The 50% paw withdrawal threshold was determined in grams by the Dixon nonparametric test.[42] The protocol was repeated until three changes in behaviour occurred.

Data and statistical analyses

All experiments were randomized. Data are expressed as the mean ± SEM of the number of indicated experiments. All sample sizes were chosen based on our previous studies. In all experiments in which

a significant result was obtained, the F test was followed by Bonferroni's post-hoc test for multiple comparisons to compare with the control group. The applied statistical tests are specified in each figure legend.

ACKNOWLEDGEMENTS

We thank the Support Unit of the Chimiothèque Nationale (P. Jauffret, K. Tan; CNRS UAR 3035, Montpellier) and local compound library managers (B. Didier, LIT-UMR7200 and PCBIS-UAR3286, Illkirch; J. C. Jullian, BIOCIS-UMR8076, Chatenay-Malabry; C. Beauvineau, Institut Curie-UMR9187, Orsay; L. Robin, ICOA-UMR6005, Orléans; R. Alves de Sousa, LCBPT-UMR8601, Paris; A. Comte, ICBMS-UMR5246, Lyon; P. Suzanne, CERMN-EA4258, Caen) for providing with powder samples of primary hits. We thank Dr. Cyril Rivat (INM, Montpellier) for advises on in vivo experiments, and the different technical platforms of the Institut des Neurosciences de Montpellier (INM), notably the animal care facility and the functional exploration platform. This work was supported by CNRS, INSERM, Universities of Montpellier and Strasbourg, BIODOL Therapeutics, and grants from the National Research Agency (ANR-15-CE18-0009-01, ANR-18-CE18-0020-03).

CONFLICTS OF INTEREST

J.P.-L. is currently a full-time employee at BIODOL Therapeutics. P.S., J.V., and D.R. are inventors of patents claiming FLT3 inhibitors and their use for the treatment of neuropathic pain and are co-founders of BIODOL Therapeutics. The remaining authors declare no competing interests.

REFERENCES

1. Manning, G.; Whyte, D. B.; Martinez, R.; Hunter, T.; Sudarsanam, S., The Protein Kinase Complement of the Human Genome. *Science,* **2002,** *298*, 1912-1934.
2. Trenker, R.; Jura, N., Receptor Tyrosine Kinase Activation: From the Ligand Perspective. *Curr Opin Cell Biol,* **2020,** *63*, 174-185.
3. Lemmon, M. A.; Schlessinger, J., Cell Signaling by Receptor Tyrosine Kinases. *Cell,* **2010,** *141*, 1117-1134.
4. Bromann, P. A.; Korkaya, H.; Courtneidge, S. A., The Interplay between Src Family Kinases and Receptor Tyrosine Kinases. *Oncogene,* **2004,** *23*, 7957-7968.
5. Yamaoka, T.; Kusumoto, S.; Ando, K.; Ohba, M.; Ohmori, T., Receptor Tyrosine Kinase-Targeted Cancer Therapy. *Int J Mol Sci,* **2018,** *19*.
6. Longo, F. M.; Massa, S. M., Small-Molecule Modulation of Neurotrophin Receptors: A Strategy for the Treatment of Neurological Disease. *Nat Rev Drug Discov,* **2013,** *12*, 507-525.
7. O'Farrell, A. M.; Abrams, T. J.; Yuen, H. A.; Ngai, T. J.; Louie, S. G.; Yee, K. W. H.; Wong, L. M.; Hong, W.; Lee, L. B.; Town, A.; Smolich, B. D.; Manning, W. C.; Murray, L. J.; Heinrich, M. C.; Cherrington, J. M., SU11248 Is a Novel FLT3 Tyrosine Kinase Inhibitor with Potent Activity in Vitro and in Vivo. *Blood,* **2003,** *101*, 3597-3605.
8. Bhullar, K. S.; Lagaron, N. O.; McGowan, E. M.; Parmar, I.; Jha, A.; Hubbard, B. P.; Rupasinghe, H. P. V., Kinase-Targeted Cancer Therapies: Progress, Challenges and Future Directions. *Mol Cancer,* **2018,** *17*, 48.
9. Hartmann, J. T.; Haap, M.; Kopp, H. G.; Lipp, H. P., Tyrosine Kinase Inhibitors - a Review on Pharmacology, Metabolism and Side Effects. *Curr Drug Metab,* **2009,** *10*, 470-481.
10. Gharwan, H.; Groninger, H., Kinase Inhibitors and Monoclonal Antibodies in Oncology: Clinical Implications. *Nat Rev Clin Oncol,* **2016,** *13*, 209-227.
11. Ferrara, N.; Hillan, K. J.; Gerber, H. P.; Novotny, W., Discovery and Development of Bevacizumab, an Anti-VEGF Antibody for Treating Cancer. *Nat Rev Drug Discov,* **2004,** *3*, 391-400.

12. Hudis, C. A., Drug Therapy: Trastuzumab - Mechanism of Action and Use in Clinical Practice. *New Engl J Med,* **2007,** *357*, 39-51.
13. Hernandez, I.; Bott, S. W.; Patel, A. S.; Wolf, C. G.; Hospodar, A. R.; Sampathkumar, S.; Shrank, W. H., Pricing of Monoclonal Antibody Therapies: Higher If Used for Cancer? *Am J Manag Care,* **2018,** *24*, 109-112.
14. De Smet, F.; Christopoulos, A.; Carmeliet, P., Allosteric Targeting of Receptor Tyrosine Kinases. *Nat Biotechnol,* **2014,** *32*, 1113-1120.
15. Cazorla, M.; Premont, J.; Mann, A.; Girard, N.; Kellendonk, C.; Rognan, D., Identification of a Low-Molecular Weight TrkB Antagonist with Anxiolytic and Antidepressant Activity in Mice. *J Clin Invest,* **2011,** *121*, 1846-1857.
16. Bono, F.; De Smet, F.; Herbert, C.; De Bock, K.; Georgiadou, M.; Fons, P.; Tjwa, M.; Alcouffe, C.; Ny, A.; Bianciotto, M.; Jonckx, B.; Murakami, M.; Lanahan, A. A.; Michielsen, C.; Sibrac, D.; Dol-Gleizes, F.; Mazzone, M.; Zacchigna, S.; Herault, J. P.; Fischer, C.; Rigon, P.; Ruiz de Almodovar, C.; Claes, F.; Blanc, I.; Poesen, K.; Zhang, J.; Segura, I.; Gueguen, G.; Bordes, M. F.; Lambrechts, D.; Broussy, R.; van de Wouwer, M.; Michaux, C.; Shimada, T.; Jean, I.; Blacher, S.; Noel, A.; Motte, P.; Rom, E.; Rakic, J. M.; Katsuma, S.; Schaeffer, P.; Yayon, A.; Van Schepdael, A.; Schwalbe, H.; Gervasio, F. L.; Carmeliet, G.; Rozensky, J.; Dewerchin, M.; Simons, M.; Christopoulos, A.; Herbert, J. M.; Carmeliet, P., Inhibition of Tumor Angiogenesis and Growth by a Small-Molecule Multi-FGF Receptor Blocker with Allosteric Properties. *Cancer Cell,* **2013,** *23*, 477-488.
17. Kappert, F.; Sreeramulu, S.; Jonker, H. R. A.; Richter, C.; Rogov, V. V.; Proschak, E.; Hargittay, B.; Saxena, K.; Schwalbe, H., Structural Characterization of the Interaction of the Fibroblast Growth Factor Receptor with a Small Molecule Allosteric Inhibitor. *Chemistry,* **2018,** *24*, 7861-7865.
18. Grither, W. R.; Longmore, G. D., Inhibition of Tumor-Microenvironment Interaction and Tumor Invasion by Small-Molecule Allosteric Inhibitor of DDR2 Extracellular Domain. *Proc Natl Acad Sci U S A,* **2018,** *115*, E7786-E7794.

19. Rivat, C.; Sar, C.; Mechaly, I.; Leyris, J. P.; Diouloufet, L.; Sonrier, C.; Philipson, Y.; Lucas, O.; Mallie, S.; Jouvenel, A.; Tassou, A.; Haton, H.; Venteo, S.; Pin, J. P.; Trinquet, E.; Charrier-Savournin, F.; Mezghrani, A.; Joly, W.; Mion, J.; Schmitt, M.; Pattyn, A.; Marmigere, F.; Sokoloff, P.; Carroll, P.; Rognan, D.; Valmier, J., Inhibition of Neuronal FLT3 Receptor Tyrosine Kinase Alleviates Peripheral Neuropathic Pain in Mice. *Nat Commun,* **2018,** *9*, 1042.
20. Derry, S.; Bell, R. F.; Straube, S.; Wiffen, P. J.; Aldington, D.; Moore, R. A., Pregabalin for Neuropathic Pain in Adults. *Cochrane Db Syst Rev,* **2019**.
21. Moore, R. A.; Derry, S.; Aldington, D.; Cole, P.; Wiffen, P. J., Amitriptyline for Neuropathic Pain in Adults. *Cochrane Db Syst Rev,* **2015**.
22. Cavalli, E.; Mammana, S.; Nicoletti, F.; Bramanti, P.; Mazzon, E., The Neuropathic Pain: An Overview of the Current Treatment and Future Therapeutic Approaches. *Int J Immunopathol Pharmacol,* **2019,** *33*, 2058738419838383.
23. Degorce, F.; Card, A.; Soh, S.; Trinquet, E.; Knapik, G. P.; Xie, B., Htrf: A Technology Tailored for Drug Discovery - a Review of Theoretical Aspects and Recent Applications. *Curr Chem Genomics,* **2009,** *3*, 22-32.
24. Zhang, J. H.; Chung, T. D. Y.; Oldenburg, K. R., A Simple Statistical Parameter for Use in Evaluation and Validation of High Throughput Screening Assays. *J Biomol Screen,* **1999,** *4*, 67-73.
25. Mahuteau-Betzer, F., [the French National Compound Library: Advances and Future Prospects]. *Med Sci (Paris),* **2015,** *31*, 417-422.
26. BDT121 Is a Close Analog of BDT001 with Comparable FLT3 NAM Properties and an in Vitro Potency of 10 µm.
27. Hopkins, A. L.; Groom, C. R.; Alex, A., Ligand Efficiency: A Useful Metric for Lead Selection. *Drug Discov Today,* **2004,** *9*, 430-431.
28. Lipinski, C. A., Rule of Five in 2015 and Beyond: Target and Ligand Structural Limitations, Ligand Chemistry Structure and Drug Discovery Project Decisions. *Adv Drug Deliv Rev,* **2016,** *101*, 34-41.

29. Zarrinkar, P. P.; Gunawardane, R. N.; Cramer, M. D.; Gardner, M. F.; Brigham, D.; Belli, B.; Karaman, M. W.; Pratz, K. W.; Pallares, G.; Chao, Q.; Sprankle, K. G.; Patel, H. K.; Levis, M.; Armstrong, R. C.; James, J.; Bhagwat, S. S., AC220 Is a Uniquely Potent and Selective Inhibitor of FLT3 for the Treatment of Acute Myeloid Leukemia (Aml). *Blood,* **2009,** *114*, 2984-2992.

30. Karl, K.; Hristova, K., Pondering the Mechanism of Receptor Tyrosine Kinase Activation: The Case for Ligand-Specific Dimer Microstate Ensembles. *Curr Opin Struct Biol,* **2021,** *71*, 193-199.

31. Rault, S.; Lancelot, J.-C.; Prunier, H.; Robba, M.; Delagrange, P.; Renard, P.; G., A., 5-HT3 Pyrrolopyrazine Derivatives, EP0623620, 1994.

32. Contreras, J. M.; Rival, Y. M.; Chayer, S.; Bourguignon, J. J.; Wermuth, C. G., Aminopyridazines as Acetylcholinesterase Inhibitors. *J. Med. Chem.,* **1999,** *42*, 730-741.

33. Chan, C.; Yin, H.; Garforth, J.; McKie, J. H.; Jaouhari, R.; Speers, P.; Douglas, K. T.; Rock, P. J.; Yardley, V.; Croft, S. L.; Fairlamb, A. H., Phenothiazine Inhibitors of Trypanothione Reductase as Potential Antitrypanosomal and Antileishmanial Drugs. *J Med Chem,* **1998,** *41*, 148-156.

34. Waksman, G.; Oswald, R.; Changeux, J. P.; Roques, B. P., Synthesis and Pharmacological Activity on Electrophorus Electricus Electroplaque of Photoaffinity Labelling Derivatives of the Non-Competitive Blockers Di- and Tri-Methisoquin. *FEBS Lett,* **1980,** *111*, 23-28.

35. Casimiro-Garcia, A.; Trujillo, J. I.; Vajdos, F.; Juba, B.; Banker, M. E.; Aulabaugh, A.; Balbo, P.; Bauman, J.; Chrencik, J.; Coe, J. W.; Czerwinski, R.; Dowty, M.; Knafels, J. D.; Kwon, S.; Leung, L.; Liang, S.; Robinson, R. P.; Telliez, J. B.; Unwalla, R.; Yang, X.; Thorarensen, A., Identification of Cyanamide-Based Janus Kinase 3 (Jak3) Covalent Inhibitors. *J Med Chem,* **2018,** *61*, 10665-10699.

36. El-Ahmad, Y.; Reynaud, P., Sur le Mécanisme de la Réaction de Meth-Cohn-Tarnowski de Préparation des Thiocoumarines. *J Heterocycl Chem,* **1988,** *25*, 711-714.

37. Kaliyaperumal, S.; Wilson, K.; Aeffner, F.; Dean, C., Jr., Animal Models of Peripheral Pain: Biology Review and Application for Drug Discovery. *Toxicol Pathol,* **2020,** *48*, 202-219.

38. Chaplan, S. R.; Bach, F. W.; Pogrel, J. W.; Chung, J. M.; Yaksh, T. L., Quantitative Assessment of Tactile Allodynia in the Rat Paw. *J Neurosci Methods,* **1994,** *53*, 55-63.

39. Valencia, C.; Dujet, C.; Margathe, J. F.; Iturrioz, X.; Roux, T.; Trinquet, E.; Villa, P.; Hibert, M.; Dupuis, E.; Llorens-Cortes, C.; Bonnet, D., A Time-Resolved Fret Cell-Based Binding Assay for the Apelin Receptor. *ChemMedChem,* **2017,** *12*, 925-931.

40. Elziere, L.; Sar, C.; Venteo, S.; Bourane, S.; Puech, S.; Sonrier, C.; Boukhadaoui, H.; Fichard, A.; Pattyn, A.; Valmier, J.; Carroll, P.; Mechaly, I., Camkk-Camk1a, a New Post-Traumatic Signalling Pathway Induced in Mouse Somatosensory Neurons. *PLoS One,* **2014,** *9*, e97736.

41. Verstraete, K.; Koch, S.; Ertugrul, S.; Vandenberghe, I.; Aerts, M.; Vandriessche, G.; Thiede, C.; Savvides, S. N., Efficient Production of Bioactive Recombinant Human FL Ligand in E. Coli. *Protein J,* **2009,** *28*, 57-65.

42. Dixon, W. J., Efficient Analysis of Experimental Observations. *Annu Rev Pharmacol Toxicol,* **1980,** *20*, 441-462.

Table of Contents Graphics

Romain Hany, Jean-Philippe Leyris, Guillaume Bret, Sylvie Mallié, Chamroeun Sar, Maxime Thouaye, Abdallah Hamze, Olivier Provot, Pierre Sokoloff, Jean Valmier, Pascal Villa and Didier Rognan.